Chapter 2 Earthquake, Tsunami and Damage in Banda Aceh and Northern Sumatra

2.1 Introduction

At 00:58:53 GMT (07:58:53 local time at the epicenter), December 26th 2004, a great earthquake with a moment magnitude (M_w) of 9.0 (USGS) occurred off the west coast of northern Sumatra, Indonesia (3.307°N, 95.947°E) and generated a huge tsunami with a tsunami magnitude (M_t) of 9.1 (Abe, 2005). An earthquake of $M_w \geq 9.0$ had not occurred in this region for at least 200 years. The tsunami hit Banda Aceh (the most devastated city in the disaster), Indonesia (near the tsunami source), Thailand (about 500 km from the source), Sri Lanka (1,200 km from the source) and the southeast coast of India (about 1,500 km from the source) (Fig. 2.1). It claimed many lives and heavily damaged property and infrastructure. The figures for dead and missing reached approximately 181,700 and 51,400 respectively, as of April 8th 2005. Many people lived on low-lying coastal areas without refuge buildings and lacked tsunami knowledge and an early tsunami warning system. These three factors would be partly responsible for the great human loss of life.

This chapter reports on the real state of the earthquake, tsunami and damage at Banda Aceh and the northern part of Sumatra in Indonesia. The areas were surveyed from January 20th 2005, nearly 3 weeks after the tsunami, until January 29th 2005. Problems to be solved from a viewpoint of damage estimation are also discussed.

2.2 Field Survey

An international tsunami survey team with experts from Japan (7 persons), Indonesia (6), the United States (2) and France (2) was formed, and surveyed Banda Aceh and the northern part of Sumatra in Indonesia from 20-29th January 2005, only 3 weeks after the tsunami. The Japanese members of the field survey team in Indonesia were as follows:

Takanobu KAMATAKI (National Institute of Advanced Industrial Science and Technology)
Hideo MATSUTOMI (Akita University)
Yoshikane MURAKAMI (Kansai Electric Power Co., Inc.)
Yuichi NISHIMURA (Hokkaido University)
Tsutomu SAKAKIYAMA (Central Research Institute of Electric Power Industry)
Yuichiro TANIOKA (Hokkaido University)
Yoshinobu TSUJI (University of Tokyo) Leader of the survey team

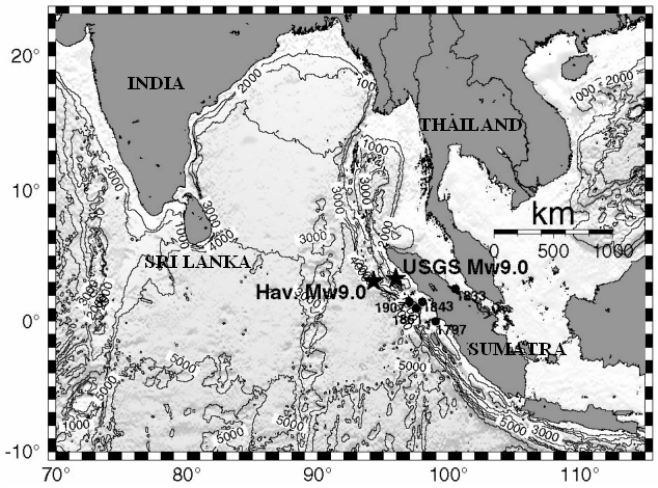

Fig. 2.1 Epicenters of the present (★) and past (●) earthquakes and bathymetry of the Indian Ocean.

Fig. 2.2 Map of Ache province in Indonesia.

Major points of the field survey:

1) Coseismic crustal deformation
2) State of tsunami attack
3) Tsunami heights and their distribution
4) Current velocity and fluid force of inundated flow (Matsutomi, 1993)
5) Tsunami deposits
6) Damage to buildings, coastal and harbor structures, oil storage tanks and so on

The surveyed areas are shown in Figs. 2.7 and 2.8 (enlarged). The areas are Banda Aceh, Lhoknga on the west coast, Sigli on the east coast, and both the north and south coasts of Weh Island.

2.3 Earthquake, tsunami and damage at Banda Aceh and the environs

2.3.1 Coseismic crustal deformation survey

The Sumatra-Andaman earthquake on 26 December 2004 was the largest in the world since the 1964 great Alaska earthquake. The aftershock area extended from northwest of Sumatra Island to the Andaman Islands. The total length of the aftershock area was over 1,200 km. The mechanism of the earthquake according to the Harvard CMT catalog indicates thrust type faulting (strike=329°, dip=8°, rake=110°). This suggests that the earthquake was an under-thrusting plate boundary event due to the subduction of the Indian-Australian plate beneath the Eurasian plate.

The teleseismic waveform study by Ammon et al. (2005) showed that the rupture expanded at a speed of about 2.5 km/s in a north northwest direction, extending 1,200 to 1,300 km along the Andaman trough. They also suggested that the some slip in the northern 400 to 500 km of the aftershock zone occurred on a time scale beyond the seismic band. The Earth's free oscillation study by Park et al. (2005) shows that the seismic moment of the earthquake was 6.5×10^{22} Nm (M_w 9.15), with a rupture duration of 600 seconds. Lay et al. (2005) also indicated that additional slow slip occurred in the north over a time scale of 50 minutes or longer.

Photo 2.1 The rice field was submerged near the coast at Peukan Bada.

Photo 2.2 Trees were submerged at Leupung (left) and Lhok Nga (right).

All of the above results suggest that the unusual slow slip nature was a part of the source process of the 2004 Sumatra-Andaman earthquake. However, the qualitative analysis of the slow slip nature using seismological data is limited, as shown by Ammon et al. (2005). The crustal deformation and tsunami waveform data were essential for studying the slow source processes of the event and tsunami generation.

Our international tsunami survey team began a 10-day investigation in Ache province in Indonesia from January 20, 2005 (Fig. 2.2). Coseismic crustal deformation data and tsunami waveforms data were also collected during the survey.

2.3.1.1 Coseismic crustal deformation data and tsunami waveform data

In Banda Ache City, a geodetic survey was conducted in 2002 by the local government in order to construct a drainage system. The survey data was available from the local government. Although the tsunami destroyed most of the structures near the coast, several survey points measured in 2002 remained and were re-measured during our survey. The result showed that subsidence of 20-60 cm occurred in Banda Ache City (Fig. 2.2).

At Peukan Bada, located to the west of the Banda Ache city, a rice field near the coast was submerged after the earthquake (see photo 2.1.). Because the rice field was originally above the high tide level, we measured the ground level of the rice field from the high tide level. It suggested that subsidence of more than 20 cm had occurred due to the earthquake.

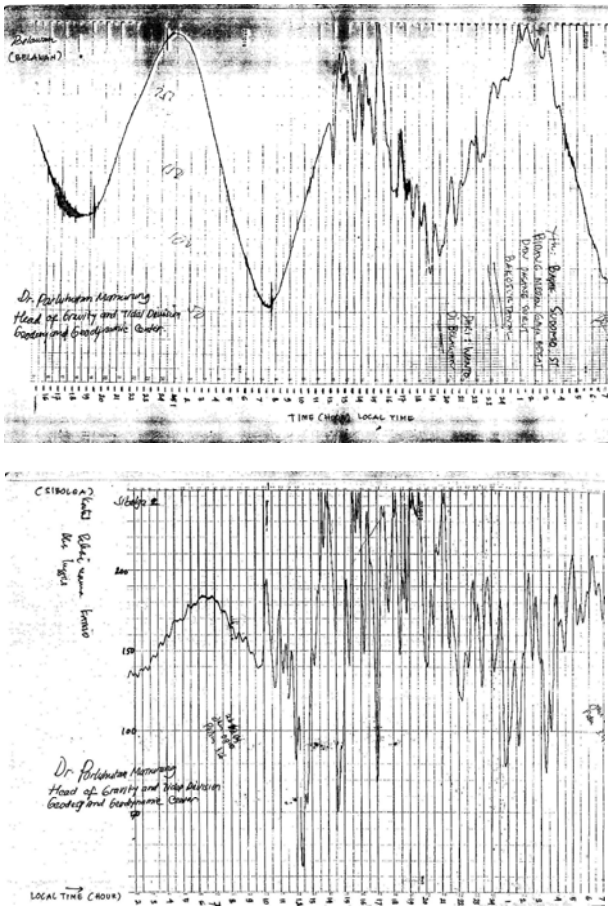

Fig. 2.3 Tsunami waveforms at Belawan (upper) and Sibolga (lower).

At Lhok Nga and Leupung, located along the west coast of Ache province, some of the trees along the coast were also submerged after the earthquake, as shown in Photo 2.2. We measured ground levels at the roots of the trees from the high tide levels. It suggested that subsidence of more than 1.5 m had occurred there. The subsidence could be due to erosion caused by the tsunami. Therefore, the subsidence due to the earthquake might be smaller than our estimates in this area.

Analog tsunami waveforms recorded at two tide gauges, Sibolga and Belawan, were collected during the survey (Fig. 2.3).

2.3.1.2 Analysis

Tanioka et al. (2005) studied the source process of the 2004 Sumatra-Andaman earthquake using the above coseismic crustal deformation data, tsunami waveforms observed at two tide gauges, and the data collected by other surveys. Additional data included: the tsunami waveform observed at Colombo by the National Aquatic Resources Agency in Sri Lanka; tsunami waveforms observed at Port Blair and Vishakhapatnam by the National Institute of Ocean Technology and the National Geophysical Research Institute in India; and the coseismic crustal deformation data on Simeulue Island as observed by the other international tsunami survey team in Indonesia.

The tsunami waveforms were numerically computed using the actual bathymetry. The linear long wave equations with the Coriolis force were solved using finite-difference calculations on a staggered grid system. The grid spacing for the Indian Ocean is 1 min x 1 min. Near the tide gauges, the grid spacing is 20 sec x 20 sec. The fault geometry is shown in Fig. 2.4. The slip distribution and the rupture velocity were estimated by trial and error.

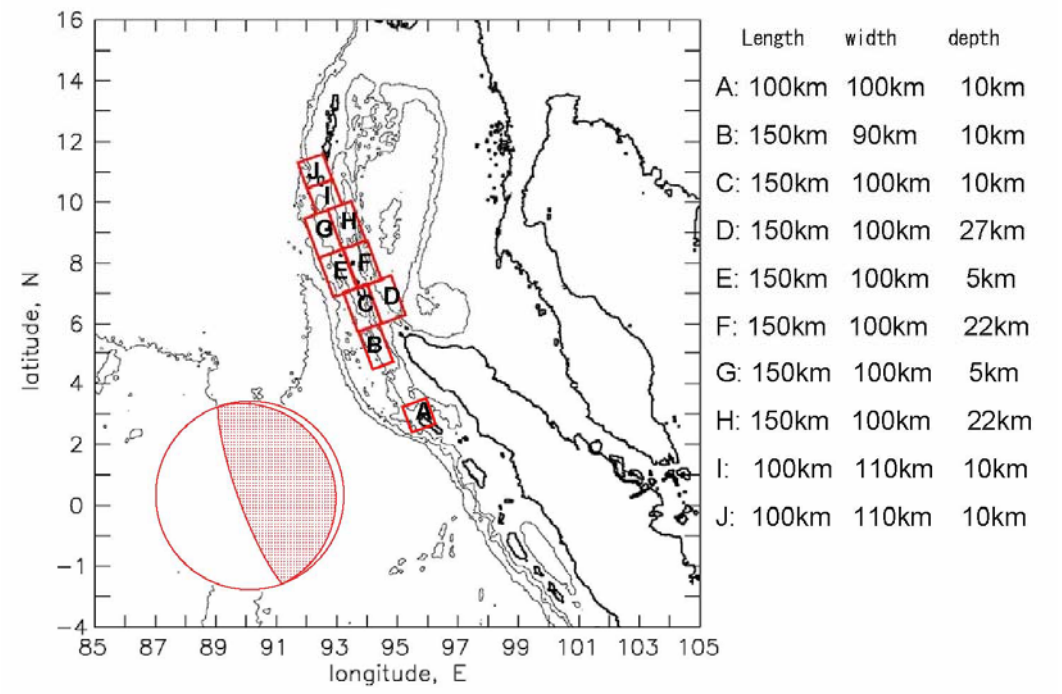

Fig. 2.4 Fault geometry of the 2004 Sumatra-Andaman earthquake.

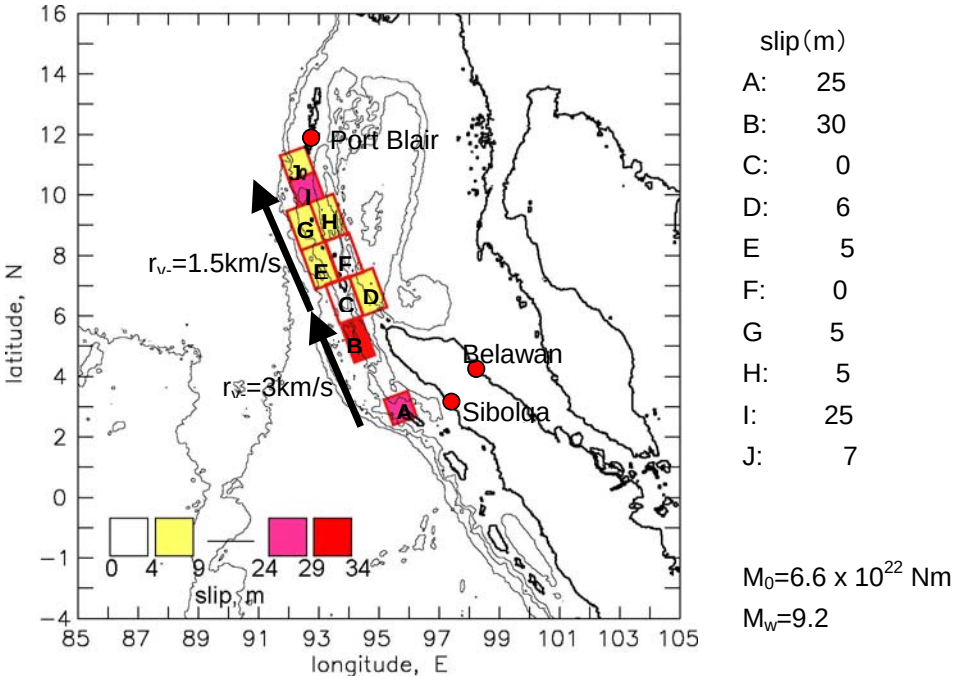

Fig. 2.5 The slip distribution of the 2004 Sumatra-Andaman earthquake.

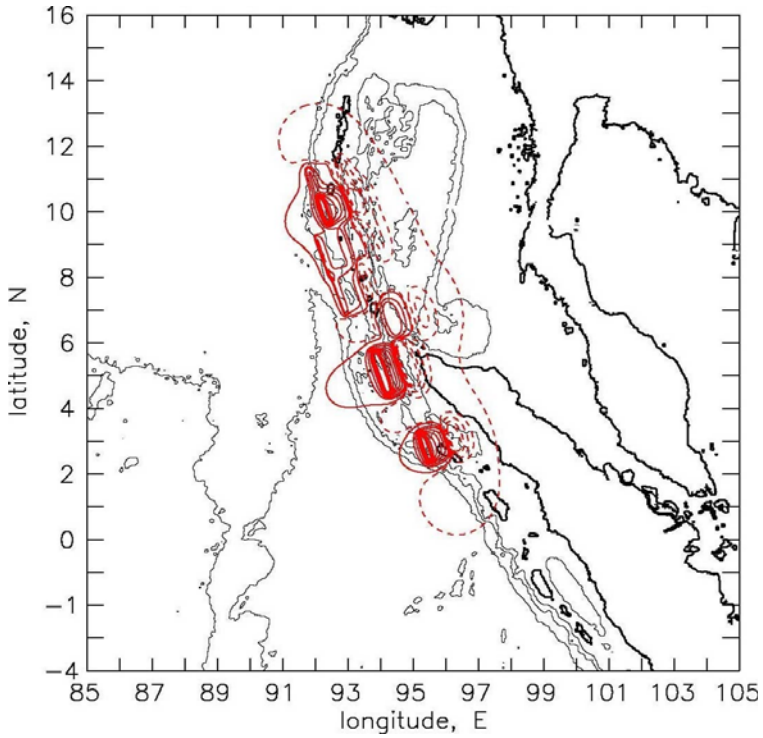

Fig. 2.6 Coseismic vertical deformations due to the Sumatra-Andaman earthquake. Dash lines show the subsidence and solid red lines show the uplift.

Photo 2.3 A clock found near the Great Mosque located in the central part of Banda Aceh.

2.3.1.3 Results

One of the best results which can explain the above data is shown in Fig. 2.5. The rupture velocities at the southern part and northern part were 3 km/s and 1.5 km/s, respectively. It indicates that the northern part was a slow rupture. The largest slip of 30 m was estimated on the subfault located off the west coast of Ache province. The large tsunami off the west coast of Ache province was probably due to this large slip on the subfault. The total seismic moment was 6.6×10^{22} Nm which is similar to the other results estimated from the seismological studies (Ammon et al., 2005, Park et al, 2005). The observed subsidence at Banda Ache (20-60 cm), Peukan Bada (>20 cm), Lhok Nga and Leupung (>1.5 m), are well explained by this result as shown in Fig. 2.6.

2.3.2 State of tsunami attack

According to eyewitnesses at Ulee Lheue in Band Aceh located at ★ in Fig. 2.8, the first tsunami reached shore 15-20 minutes after the earthquake, the time interval between the first and second tsunamis was 15-20 minutes, and the second was bigger than the first. The eyewitness report that the second was bigger than the first is the same as that in Khao Lak and Phuket Island in southern Thailand (Matsutomi et al., 2005).

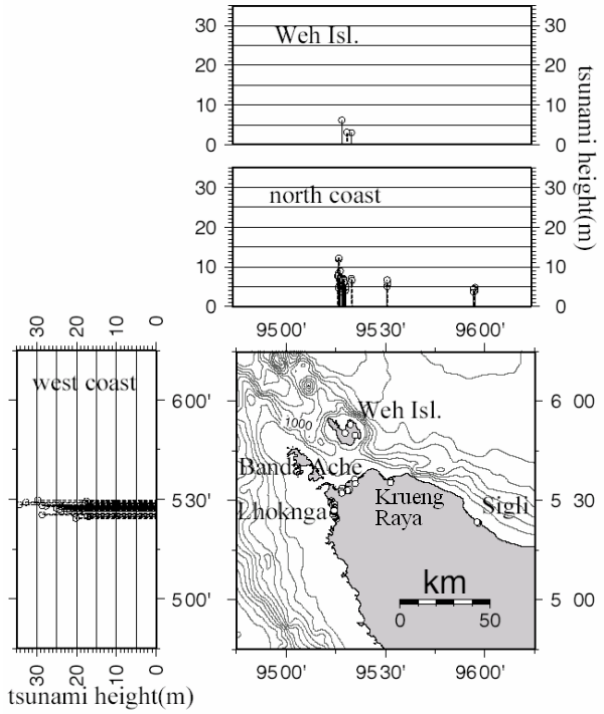

Fig. 2.7 Survey areas and tsunami (run-up) height distribution.

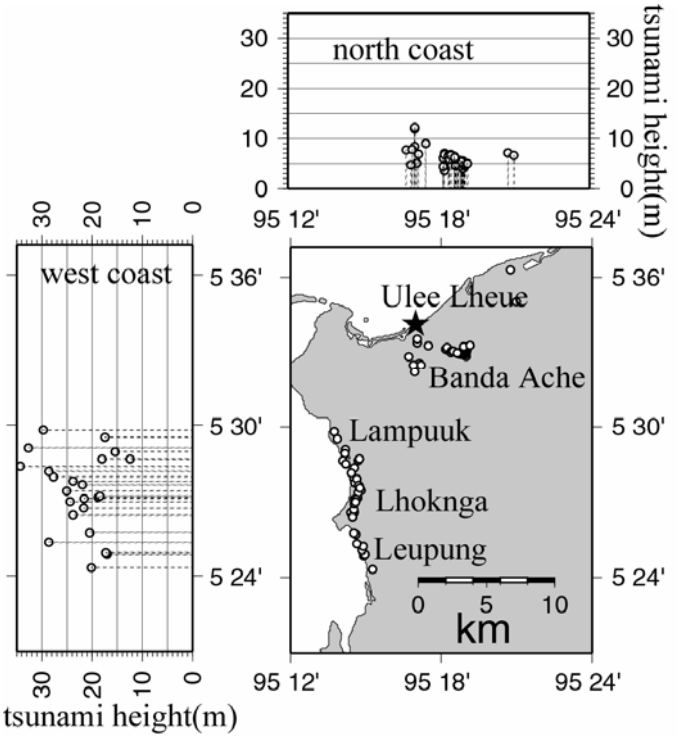

Fig. 2.8 Survey areas and tsunami (run-up) height distribution (enlarged).

The origin time of the earthquake was 07:59 on December 26th 2004. If the waveform is assumed to be a trigonometric function, the fastest and latest arrival times of the second tsunami are estimated as follows:

The fastest case: 07:59 + 15 minutes + 15minutes + 15/4 minutes ≅ 08:33

The latest case: 07:59 + 20 minutes + 20minutes + 20/4 minutes ≅ 08:44

The video of inundated flow taken at Putri (Photo 2.6), located 2.3 km inland, shows the scene from 08:50:23 (Sakakiyama et al., 2005). As the inundated flow in the video seems to be the peak period of the second tsunami, it may be judged that the eyewitnesses are fairly sound.

A clock shown in Photo 2.3 was found about 4 km inland in the central part of Banda Aceh. It indicates 08:12. Whether the clock was right is not clear.

2.3.3 Tsunami heights and their distribution

Tsunami (run-up) heights in Banda Aceh and the environs are shown in Figs. 2.7 and 2.8. These are corrected to ones above sea level at the time of tsunami attack.

The maximum height of the tsunami was measured at Leupung, located on the west coast of the northern tip of Sumatra, near Banda Aceh, and reached more than 30 m. Roughly speaking, tsunami heights on other coasts were 15-30 m on the west coast, 6-12 m on the Banda Aceh coast, about 6 m on the Krueng Raya coast – where 3 oil tanks floated out – and about 5 m on the Sigli coast. The tsunami heights in Weh Island were 3-6 m on the north coast directly facing the tsunami source and about 3 m on the opposite side of the coast.

The tsunami height on the Banda Aceh coast is lower than half of that on the west coast. Even within the Banda Aceh coast, the tsunami height reduced by half from 12 m at Ulee Lheue to 6 m a further

8 km to the northeast. One of the reasons seems to be that there is archipelago between Lhoknga and Banda Aceh (Fig. 2.8).

The tsunami advanced about 4 km inland at Banda Aceh. Within 2-3 km from the shoreline, houses, except for strongly-built reinforced concrete ones with brick walls (Photo 2.4), which seemed to have been partially damaged by the earthquake before the tsunami attack, were completely swept away or destroyed by the tsunami. Inundation depth (Photo 2.4) and estimated current velocity at a distance of about 0.9 km inland from the shoreline were nearly 5 m and 8 m/s, respectively. The tsunami height reduced from 12 m at Ulee Lheue to about 5 m (inundation depth of 1.6 m. See Photo 2.9) at the Great Mosque, located in the central part of Banda Aceh.

Location of asperity in the focal region of the earthquake is not well known (Yagi, 2005). The huge tsunamis on the west coast of northern Sumatra and Khao Lak in southern Thailand (Matsutomi et al., 2005) would have a big effect on determining the focal process of the earthquake, the initial waveform of the tsunami in the source region and so on.

2.3.4 Current velocity and fluid force of inundated flow

Data on inundation depths and current velocities in heavily affected areas were energetically collected to discuss the strength and criterion for the destruction of buildings, which would be useful, for example, to estimate tsunami damage and to build refuge buildings.

Figures 2.9(a) and 2.9(b) show the relation between the inundation depth h and the current velocity u, where the subscripts f and r distinguish between the front and rear sides of structure such as houses. They are nondimensionalized by the gravitational acceleration g and the nearest tsunami (run-up) height R. The filled circles and triangles are data collected from this tsunami, and the opened circles are data collected from past tsunamis. The solid lines in Figs. 2.9(a) and 2.9(b) are Eqs. (1) and (2) for two different values of F_r and envelopes for the field data (Matsutomi and Iizuka, 1998).

$$\frac{u}{\sqrt{gR}} = \sqrt{\frac{2C_v^2 F_r^2}{F_r^2 + 2C_v^2}} \sqrt{\frac{h_f}{R}} \tag{1}$$

$$\frac{u}{\sqrt{gR}} = F_r \sqrt{\frac{h_r}{R}} \tag{2}$$

where C_v (=0.8-0.9) is the velocity coefficient and F_r (= $u/\sqrt{gh_r}$) the Froude number. From the figures, it is clear that the data from this tsunami has the same tendency as that from past tsunamis.

Photos 2.4-2.6 show examples of variation of the inundation depth, current velocity and so on due to the distance from shoreline. The judgments of degree of damage to houses are based on the criterion of destruction defined by Matsutomi and Shuto (1994).

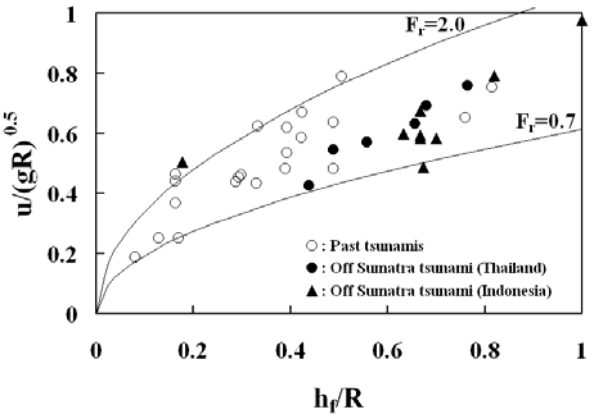

(a) Case used inundation depth on the front side

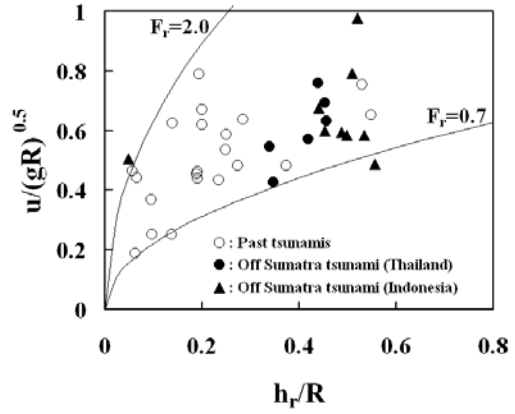

(b) Case used inundation depth on the rear side

Fig. 2.9 Relation between nondimensionalized inundation depth and current velocity.

These are all examples for a low-lying coastal area in Banda Aceh. The distance, inundation depth, current velocity and drag force F (dominant force (Matsutomi et al., 2004)) per unit area are (0.9 km, 4.9 m, 7.7 m/s, 6.2 tf/m^2 (6.1×10^4 Pa)), (1.3 km, 4.0 m, 5.2 m/s, 2.9 tf/m^2 (2.8×10^4 Pa)) and (1.5 km, 3.9 m, 5.8 m/s, 3.5 tf/m^2 (3.4×10^4 Pa)), respectively. The current velocity and drag force are estimated by the following equations:

$$u = \sqrt{2g(h_f - h_r)} \tag{3}$$

$$F = \rho C_D u^2 a/2 \cong \rho q u \tag{4}$$

where ρ is the density of seawater, C_D (≅2) the drag coefficient, a the unit area and q the flow rate per unit area.

The current velocity was estimated by using tsunami traces left on a hill (Photo 2.7). The current velocity of about 16 m/s and drag force of about 26.9 tf/m^2 (2.6×10^5 Pa) were estimated in front of a cement factory at Leupung. Traces on a hill seem to be useful to estimate the current velocity in a huge tsunami.

2.3.5 Tsunami deposit survey

The Sumatra-Andaman earthquake on 26 December 2004 was the largest in the world since the 1964 great Alaska earthquake. Recently, tsunami deposit studies have became important for estimating recurrence intervals of great earthquakes or identifying tsunami inundation areas (Atwater, 1987, Nanayama et al., 2004, etc). The tsunami deposit survey of the Sumatra-Andaman earthquake will provide a variable opportunity to compare the distribution of tsunami deposits with tsunami heights or inundation areas.

Photo 2.4 Partially damaged family house located about 0.9 km inland in Banda Aceh. Left side is shore and right side inland. Numerals indicate inundation depths.

Photo 2.5 Partially damaged family house about 1.3 km inland in Banda Aceh. Left side is shore and right side inland. Numerals indicate inundation depths.

Photo 2.6 Partially damaged family house about 2.3 km inland in Banda Aceh. Left side is shore and right side inland. Numerals indicate inundation depths.

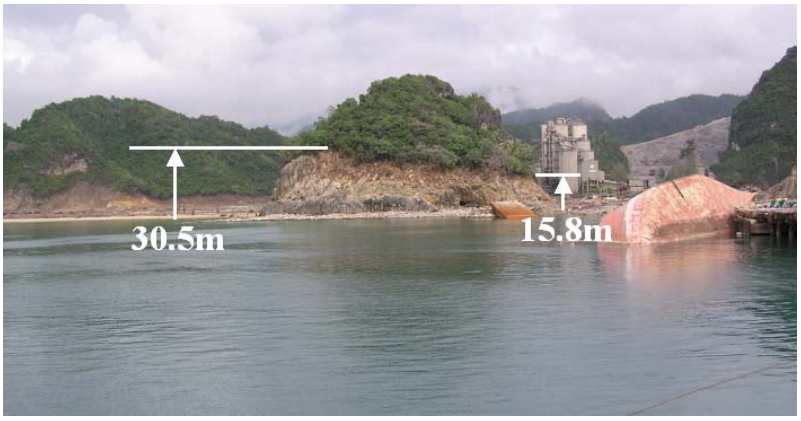

Photo 2.7 Tsunami traces left on a hill at Leupung, located on the west coast of the northern tip of Sumatra. The maximum tsunami height of nearly 35 m was measured near here.

Photo 2.8 A coral stone deposited by the tsunami at Lhok Nga.

Photo 2.9 Tsunami deposits (sand) in the trenches along the survey line at Lhok Nga.

2.3.5.1 Tsunami deposits

In the tsunami inundation area, we found a large amount of debris from houses and other constructions destroyed by the tsunami. In addition, we found coral stones with diameters of more than 1 m carried by the tsunami from the ocean (Photo 2.8), and a large amount of sand from the beach. These are called “Tsunami deposits”.

The detailed distribution of tsunami deposits – i.e sand – was surveyed along three lines from the beach going inland. These survey lines were located at Lhok Nga and Leupung. Along the lines, several trenches are made to observe the structure of the tsunami deposits and to measure thicknesses of sand layers (Photo 2.9). The distance between trenches is between 100-50 m.

2.3.5.2 Results

The maximum thickness of the tsunami deposits of sand we observed along the three lines was about 70 cm. Most of them were composed of beach-sand including shells and corals. The rip-up clasts from the original soil deposits, diameters of a few mm, were also found in the tsunami deposits. The tsunami deposits can be separated into several units, and there are structures indicating that the upper unit eroded the lower unit (Photo 2.9). This suggests that the tsunami deposits are created by tsunami waves which deposited sands and eroded sands repeatedly. The normal graded structure inside a unit is also found in most of the units (Photo 2.9). In general, the thickness of the tsunami deposits decreases when the distance from the coast increases, although the thickness of the tsunami deposits is very much affected by the local topography.

Flow directions of the tsunami were also estimated from the direction of grasses or trees pushed down by the tsunami and the distribution of debris around large trunks of trees. The flow direction was found to be almost perpendicular to the coastline.

2.4 Problems from a viewpoint of damage estimation

Initial tsunami waveform and on-offshore tsunamis are big problems to be solved. Examples of the problems, except for dynamic analysis of tsunami generation and detection of initial waveforms in source regions are as follows:

1) Is it possible to estimate this great earthquake with M_w=9.0 with the conventional method developed by the Headquarters for Earthquake Research Promotion in Japan (Matsutomi et al., 2005).
2) Improvement of the present tsunami warning system to cope with great earthquakes and huge tsunamis (see Chapter 4).
3) Refinement of the criterion for destruction of buildings and influence of ground erosion on them (Matsutomi et al., 2005).
4) Generalization of methods of estimating current velocity (Photos 2.4-2.6).
5) Method of estimating current velocity by use of a hill (Photo 2.7).
6) Increase of destructive force and current velocity of inundated flow with floating bodies.

7) Effect of coastal forest on reducing tsunami energy.

The problem 6) is discussed in the following section. In the problem 7) governing equations for inundated flow in vegetated area, similarity law for trunk and effect of coastal forest based on reports of past tsunamis and laboratory experiments have been discussed, but there still remain a lot of problems to be solved, for example, similarity law for foliage and so on.

2.5 A simple theory of inundated flow with floating bodies

Inundated flows with floating bodies such as debris, driftwood, cars, bikes and boats were videotaped at Banda Aceh and drew our attention. So did the collision forces of such floating bodies. These would be also problems to be solved immediately. Matsutomi (1999) took up impulsive force due to collision of driftwood and developed a simple method of estimating it.

This section, in connection with the above impulsive force, presents a simple theory for estimating moving velocity of floating bodies, i.e. current velocity of inundated flow with floating bodies. The theory adopts the conventional bore theory regarding the floating bodies as a fluid. Although the applicability of the theory may be low, it seems to show a way to analysis of inundated flow with floating bodies.

2.5.1 Theory

Let us consider a steady bore with debris, oil and so on, and regard those as a fluid with the same density as those in the downstream region of the bore.

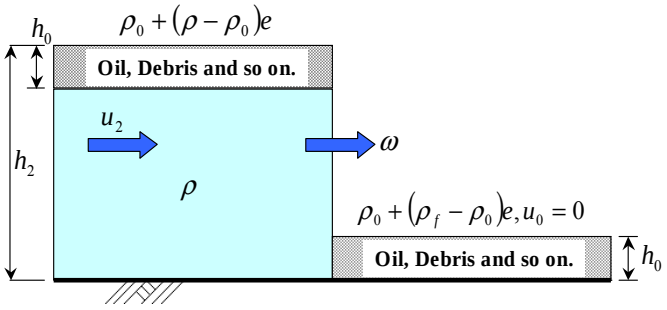

Fig. 2.10 A simplified model of inundated flow with floating bodies and definition of symbols.

The model is shown in Fig. 2.10. This figure is the case where the density of seawater is greater than that of the hypothetical fluid in the downstream region. As the vertical pressure distribution in the upstream region of the bore depends on the vertical distribution of the floating bodies, current velocity and bore propagation velocity also depend on that of the floating bodies. In this model, the floating bodies are swallowed up in the bore while maintaining their distribution in the downstream region, and then seawater gets into their void.

2.5.1.1 Continuity equation

The mass conservation law based on this model is as follows:

$$[\{\rho_0+(\rho-\rho_0)e\}h_0+\rho(h_2-h_0)](\omega-u_2)=\{\rho_0+(\rho_f-\rho_0)e\}h_0\omega \tag{5}$$

where ρ_0 is the density of floating bodies, ρ_f the density of the void part in the downstream region (zero in case of air), e the void ratio of floating bodies in the downstream region, h_2 the water depth in the upstream region, u_2 the current velocity in the upstream region, h_0 the thickness of floating bodies layer in both the upstream and downstream regions, u_0 (=0) the current velocity in the downstream region, and ω the bore (or front) propagation velocity.

The density in {} on the right hand side of Eq. (5) is the mean density of the hypothetical fluid in the downstream region. When $\rho_0=\rho_f=\rho$, Eq. (5) results in the mass conservation law of an ideal bore.

2.5.1.2 Momentum equation

Assuming the hydrostatic pressure distribution, the momentum conservation law is as follows:

$$\begin{aligned}&[\{\rho_0+(\rho-\rho_0)e\}h_0+\rho(h_2-h_0)](\omega-u_2)u_2=\rho g(h_2-h_0)^2/2\\&\quad+\{\rho_0+(\rho-\rho_0)e\}gh_2h_0-\{2(1-e)\rho_0+(\rho+\rho_f)e\}gh_0^2/2\end{aligned}\tag{6}$$

The hydrostatic pressure on the downstream side is taken into account in Eq. (6). This is reasonable for a real fluid such as oil, but there is room for reconsideration for debris and so on. If the hydrostatic pressure is ignored, the current velocity and front propagation velocity become larger than those in the case taken into account.

When $\rho_0=\rho_f=\rho$, Eq. (6) results in the momentum conservation law of an ideal bore.

2.5.1.3 Current velocity and front propagation velocity of inundated flow

Equations (5) and (6) lead to the following current velocity u_2 and front propagation velocity ω:

$$u_2=\frac{\left(\frac{\rho}{\rho_0}-\frac{\rho_f}{\rho_0}\right)e+\frac{\rho}{\rho_0}\left(\frac{h_2}{h_0}-1\right)}{\left\{1+\left(\frac{\rho}{\rho_0}-1\right)e\right\}+\frac{\rho}{\rho_0}\left(\frac{h_2}{h_0}-1\right)}\omega\tag{7}$$

$$\begin{aligned}\omega=&\sqrt{g\left[\left\{\frac{\rho_0}{\rho}+\left(1-\frac{\rho_0}{\rho}\right)e\right\}h_0+h_2-h_0\right]\Big/\left\{1+\left(\frac{\rho_f}{\rho_0}-1\right)e\right\}\left\{\left(1-\frac{\rho_f}{\rho}\right)e+\frac{h_2}{h_0}-1\right\}}\\&\times\sqrt{\frac{1}{2}\frac{\rho}{\rho_0}\left(\frac{h_2}{h_0}-1\right)^2+\left\{1+\left(\frac{\rho}{\rho_0}-1\right)e\right\}\frac{h_2}{h_0}-\frac{1}{2}\left\{2(1-e)+\left(\frac{\rho}{\rho_0}+\frac{\rho_f}{\rho_0}\right)e\right\}}\end{aligned}\tag{8}$$

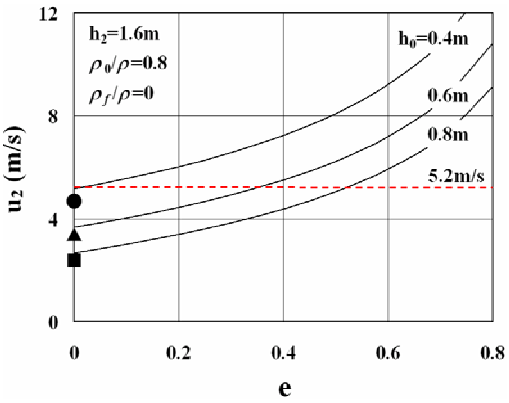

Fig. 2.11 Examples of moving velocity of floating bodies (≅ current velocity).

Photo 2.10 Inundated flow with floating bodies (just in front of the Great Mosque in Banda Aceh).

2.5.2 Example of solution

The moving velocity of floating bodies seems to be almost the same as the current velocity u_2 in a steady state. Examples of the solution of u_2 are shown in Fig. 2.11. The conditions on h_2, ρ_0/ρ and ρ_f/ρ were determined by the video picture (Photo 2.10) taken just in front of the Great Mosque located in the central part of Banda Aceh and surveying the length and height of buildings in the video picture. The dotted line in the figure denotes the moving velocity of floating bodies (≅5.2 m/s) estimated by analyzing the video picture (Sakakiyama et al., 2005). The Froude number of this flow is about 1.3. Circle (●), triangle (▲) and square (■) denote the current velocities estimated by the ideal bore theory for h_0=0.4, 0.6 and 0.8 m, respectively. The figure indicates that the present theory gives larger current velocity compared with that of inundated flow without floating bodies. As the densities of floating bodies and void part decrease, and as the void ratio increases, the front propagation velocity increases in the present theory.

Figure 2.11 denotes that when h_0=0.4 m, the theory can't explain the moving velocity of 5.2 m/s, but when h_0=0.6 and 0.8 m, the theory is possible to explain the velocity with e=0.35 and 0.52, respectively. As ρ_0 and h_0 are unknown in the Banda Aceh case, it is difficult to discuss further. Judging from the video picture, h_0 seems to be more than 0.4 m. Therefore, it may be concluded that the present theory is useful. It will be necessary to compare the theory with experimental results.

2.6 Summary

The main results in this section:

1) The rupture velocities at the southern part and northern part of the focal region were 3 km/s and 1.5 km/s, respectively. The largest slip of 30 m was estimated on the subfault located off the west coast of Ache province. A total seismic moment of 6.6×10^{22} Nm was estimated.
2) The observed subsidences were 0.2-0.6 m at Banda Aceh, >0.2 m at Peukan Bada, >1.5 m at Lhok Nga and Leupung, and these were well explained by the proposed focal process.
3) Roughly speaking, tsunami heights were 15-30 m on the west coast, 6-12 m on the Banda Aceh coast, about 6 m on the Krueng Raya coast, about 5 m on the Sigli coast and 3-6 m on Weh Island.
4) The distance from shoreline, inundation depth, estimated current velocity and estimated drag force per unit area in Banda Aceh were (0.9 km, 4.9 m, 7.7 m/s, 6.2 tf/m^2 (6.1×10^4 Pa)), (1.3 km, 4.0 m, 5.2 m/s, 2.9 tf/m^2 (2.8×10^4 Pa)) and (2.3 km, 3.9 m, 5.8 m/s, 3.5 tf/m^2 (3.4×10^4 Pa)), respectively. The estimated current velocity and drag force were (16 m/s, 27 tf/m^2 (2.6×10^5 Pa)) in front of the cement factory at Leupung and (3.6 m/s, 1.3 tf/m^2 (1.3×10^4 Pa)) in Sigli.
5) The maximum thickness of the tsunami deposits was about 0.7 m. The tsunami deposits could be separated into several units and were created by repeated tsunami waves. The normal graded structure inside a unit was also found in the most of the units.
6) Several problems from a viewpoint of damage estimation were pointed out. A simple theory for the inundated flow with floating bodies was presented.

References

Abe, K.: Revised M_t and run-up estimate for the Indian Ocean Tsunami, A quick report contributed to the tsunami-japan (tsunami bulletin board in Japan) on January 27th 2005.

Ammon, J. C., C. Ji, H. Thio, D. Robinson, S. Ni, V. Hjorleifsdottir, H. Kanamori, T. Lay, S. Das, D. Helmberger, G. Ichinose, J. Polet and D. Wald: Rupture process of the 2004 Sumatra-Andaman earthquake, *Science*, 308, 1133-1139, 2005.

Asian Tsunami Videos: Amateur Asian Tsunami Video Footage, http://www.Asiantsunamivideos.com/, referred on 2005-3-30.

Atwater, B. F.: Evidence for great Holocene earthquakes along the outer coast of Washington State, *Science*, 236, 942-944, 1987.

BBC: bbc.co.uk homepage - Home of the BBC on the Internet, http://news.bbc.co.uk/, referred on 2005-2-28.

JSCE: Quick report meeting on the 2004 Indian Ocean Tsunami held by JSCE on January 14th 2005, http://www.jsce.or.jp/ report/33/, referred on 2005-1-31. (in Japanese)

Kamataki, T. and Y. Nishimura: Field survey of the 2004 Off-Sumatra earthquake tsunami around Banda Ache, northern Sumatra, Indonesia, *Jour. of Geography*, 114, 78-82, 2005. (in Japanese)

Lay, T., H. Kanamori, C. J. Ammon, M. Nettles, S. N. Ward, R. C. Aster, S. L. Beck, S. L. Bilek, M. R. Brudzinski, R. Butler, H. R. Deshon, G. Ekstrom, K. Satake and S. Sipkin, The great Sumatra-Andaman earthquake of 26 December 2004, *Science*, 308, 1127-1132, 2005

Matsutomi, H.: Tsunami and damage in the northeast part of Flores Island, *Kaiyo Monthly*, Vol.25, No.12, pp.756-761, 1993. (in Japanese)

Matsutomi, H. and N. Shuto: Tsunami inundation depth, current velocity and damage to houses, *Proc. of Coastal Eng.*, *JSCE*, Vol.41, pp.246-250, 1994. (in Japanese)

Matsutomi, H., F. Imamura, T. Takahashi, K. Kurayoshi, K. Kobune, G. Watson, H. Rahman and N. Shuto: The 1996 Irian Jaya Earthquake Tsunami and Damage, *Proc. of Coastal Eng.*, *JSCE*, Vol.43, pp.311-315, 1996. (in Japanese)

Matsutomi, H. and H. Iizuka: Tsunami current velocity on land and a simple method of estimating it, *Proc. of Coastal Eng.*, *JSCE*, Vol.45, pp.361-365, 1998. (in Japanese)

Matsutomi, H.: A practical formula for estimating impulsive force due to driftwood and variation features of the impulsive force, *Jour. of Hydraulic, Coastal and Environmental Eng.*, *JSCE*, No.621/□-47, pp.111-127, 1999. (in Japanese)

Matsutomi, H., T. Ohmukai and K. Imai: Fluid force on a large structure due to an inundated flow caused by a tsunami, *Annual Jour. of Hydraulic Eng.*, *JSCE*, Vol.48, pp.559-564, 2004. (in Japanese)

Matsutomi, H., T. Takahashi, M. Matsuyama, K. Harada, T. Hiraishi, S. Supartid and S. Naksuksakul: The 2004 Off Sumatra Earthquake Tsunami and Damage at Khao Lak and Phuket Island in Thailand, *Proc. of Coastal Eng.*, *JSCE*, Vol.52, 2005. (in Japanese)

Nanayama, F., K. Satake, R. Furukawa, K. Shimokawa, B. F. Atwater, K. Shigeno, and S. Yamaki: Unusually large earthquakes inferred from tsunami deposits along the Kuril Trench, *Nature*, 424, 660-663, 2003.

Park, J., T. A. Song, J. Tromp, E. Okal, S. Stein, G. Roult, E. Clevede, G. Laske, H. Kanamori, P. Davis, J. Berger, C. Braitenberg, M. V. Camp, X. Lei, H. Sun, H. Xu and S. Rosat: Earth's free oscillations excited by the 26 December 2004 Sumatra-Andaman earthquake, *Science*, 308, 1139-1144, 2005

Royal Thai Navy: Tide gauge data, http://www.navy.mi.th/hydro/tsunami.htm, referred on 2005-3-30.

Sakakiyama, T., H. Matsutomi, Y. Tsuji and Y. Murakami: Comparison of Current velocities of Tsunami Inundated Flow Based on Analysis of Video Picture and Field Survey, *Abstract for the December 26, 2004 Off-Sumatra Earthquake meeting*, *Japan Assoc. for Earthquake Eng.*, pp.33-38, 2005.

Tanioka, Y., Yudhcara, T. Kusuniose and K. Satake: Analysis of a tsunami waveform and coseismic deformation for the 2004 Sumatra earthquake, *Abstract for the 2005 Japan Earth and Planetary Science Joint meeting*, J113, 2005.

Yagi, Y.: What Happened in the Focal region of the 2004 Off-Sumatra Great Earthquake?, *Abstract for the December 26, 2004 Off-Sumatra Earthquake meeting*, *Japan Assoc. for Earthquake Eng.*, pp.1-5, 2005.

Yamanaka, K.: Earthquake Research Institute homepage, Univ. of Tokyo, http://www.eri.u-tokyo.ac.jp/sanchu/Seismo_Note/2004/EIC161a.html, referred on 2005-2- 21. (in Japanese)